scientific reports

OPEN

Effect of laser fluence on the optoelectronic properties of nanostructured GaN/porous silicon prepared by pulsed laser deposition

Makram A. Fakhri[1]✉, Haneen D. Jabbar[1], Mohammed Jalal AbdulRazzaq[1], Evan T. Salim[2]✉, Ahmad S. Azzahrani[3]✉, Raed Khalid Ibrahim[4] & Raid A. Ismail[2]

In this study, the fabrication of nanostructured GaN/porous Si by pulsed laser deposition (PLD) was demonstrated. The porous silicon was prepared using laser-assisted electrochemical etching (LAECE). The structural, optical, and electrical properties of GaN films were investigated as a function of laser fluence. XRD studies revealed that the GaN films deposited on porous silicon were nanocrystalline, exhibiting a hexagonal wurtzite structure along the (100) plane. Spectroscopic property results revealed that the photoluminescence PL emission peaks of the gallium nitride over porous silicon (GaN/PSi) sample prepared at 795 mJ/mm^2 were centered at 260 nm and 624 nm. According to topographical and morphological analyses, the deposited film consisted of spherical grains with an average diameter of 178.8 nm and a surface roughness of 50.61 nm. The surface of the prepared films exhibited a cauliflower-like morphology. The main figures of merit of the nanostructured GaN/P-Si photodetectors were studied in the spectral range of 350–850 nm. The responsivity, detectivity, and external quantum efficiency of the photodetector at 575 nm under − 3 V were 19.86 A/W, 8.9 × 10^{12} Jones, and 50.89%, respectively. Furthermore, the photodetector prepared at a laser fluence of 795 mJ/mm^2 demonstrates a switching characteristic, where the rise time and fall time are measured to be 363 and 711 µs, respectively.

The category of semiconductor materials known as III-nitrides has gained popularity in recent years due to their wide and direct band gaps, as well as their capacity to create alloys like InGaN and AlGaN[1–3]. By adjusting the composition of these alloys, the band gap can be modified across the entire solar spectrum, from deep UV to IR[4–7]. GaN (gallium nitride), in particular, possesses a broad band gap of 3.4 eV and a wurtzite hexagonal structure, which results in minimal leakage currents and enables the operation of optoelectronic devices at elevated temperatures and frequencies[8–11]. GaN proves advantageous for optoelectronic applications, such as photodiodes, which find utility in diverse detection, monitoring, and control scenarios[12–15]. Furthermore, these photodiodes hold great promise for advanced uses, including military, medical, display, general illumination, and environmental monitoring applications[16–20]. Its distinctive characteristics also render GaN suitable for deployment in LEDs, solar cells, and photodetectors[21–24].

Several techniques, including pulsed laser deposition, chemical vapor deposition, and molecular beam epitaxy, have demonstrated successful outcomes in producing GaN thin films. These methods share a common objective: the fabrication of high-performance P-N and P-I-N heterojunctions within GaN films of varying thicknesses and on diverse substrates. These aspects encompass efficiency, speed, responsivity, and minimal dark current[24–29]. Notably, the pulsed laser deposition method presents a straightforward protocol, generating a substantial, well-directed material plume[30–33]. Additionally, it offers meticulous control over growth rate and is well-suited for generating thin films with strong adhesion on cost-effective substrates. Furthermore, this

[1]Laser and Optoelectronic Department, University of Technology-Iraq, Baghdad, Iraq. [2]Applied Science Department, University of Technology-Iraq, Baghdad, Iraq. [3]Electrical Engineering Department, Northern Border University, Arar, Kingdom of Saudi Arabia. [4]AlFarahidi University, Baghdad, Iraq. ✉email: mokaram_76@yahoo.com; makram.a.fakhri@uotechnology.edu.iq; evan_tarq@yahoo.com; evan.t.salim@uotechnology.edu.iq; ahmad.azzahrani@nbu.edu.sa

technique enables precise regulation of thin film properties, encompassing thickness and structure[34–36]. n contemporary semiconductor manufacturing, silicon (Si) is extensively employed due to its cost-effectiveness and compatibility with various processes. However, silicon's applicability in the infrared spectrum is limited due to its heightened reflectance and wide band gap[37–39]. These constraints have been significantly alleviated with the advancement of porous silicon (P-Si) technology[40]. P-Si enhances surface area, rendering it a suitable substrate for optoelectronic devices[41]. Furthermore, porous silicon (P-Si) exhibits favorable characteristics like robust room-temperature photoluminescence (PL), elevated chemical reactivity, rapid oxidation, affordability, and a quantum confinement effect that enhances radiative transitions[42–46]. As a result, P-Si finds utility in the fabrication of various optoelectronic devices, encompassing photodiodes, LEDs, detectors, and even biosensors[47–49]. Deposition of a film on porous silicon for photodetection applications was reported[50]. This offers the advantages of a large sensitive surface area, the formation of two junctions connected in series, increased responsivity of the porous photodetector, and improved speed of response of the photodetector. Herein, a new device has been fabricated make use the advantages of two differnt teqniques photonic cysrtal substrate and nanofilm active layer. The fabrication of a high-performance GaN/PSi photodetector via the pulsed laser deposition method under various laser fluences has been reported.

Experimental works

Preparation of porous silicon substrates

Mirror-like n-type (110) Si wafers with an electrical resistivity of 1–5 mΩ/cm and a thickness of 500 µm, which were purchased from University Wafer, Inc., USA, were utilized. Subsequently, the wafers were sectioned into rectangular pieces, each measuring 1 by 1 cm. Before initiating the photo-electrochemical etching process, the sections underwent a thorough cleaning using an ultrasonic device in ethanol (99.9% concentration, sourced from the German Honeywell company) for a duration of 5 min. The etching process was carried out at room temperature and involved the utilization of a diode laser (660 nm, 100 mW, from the Chinese Tongtool Company), a DC power supply with a voltage range of 0–30 V, and a digital multi-meter (Victor Company). This process, as depicted in Fig. 1, requires the use of a Teflon cell equipped with a cathode electrode made of 95% pure platinum and an anode electrode composed of silicon. The laser played a pivotal role in the top-down electrochemical etching technique employed for the synthesis of the porous silicon (PSi) substrates. Additionally, precise control was maintained over the etching conditions, with a designated etching time of 10 min, a consistently upheld current density of 10 mA/cm^2, and a constant concentration of hydrofluoric acid (HF) (sourced from the German company Thomas Baker) at 24%, achieved through the use of the dilution equation[51], as depicted in Eq. (1). The concentration of HF used in the etching process was consistently maintained at 24%, and the etching time was precisely set using a digital clock for a duration of 10 min[52–56]

$$C_1V_1 = C_2V_2 \tag{1}$$

where C_1, hydrofluoric acid concentration; V_1, hydrofluoric acid volume; C_2, ethanol concentration. V_2, ethanol volume.

Upon completion of the LAECE process, all synthesized P-Si substrates undergo a series of tests to identify the optimal outcome for varying current densities[58–60]. Structural properties were examined using X-ray diffraction (XRD) equipment (XRD6000 Shimadzu Company) from Japan, utilizing copper radiation with a wavelength of 1.54060 Å. Morphological parameters were evaluated at a high level of detail using German field emission scanning electron microscopy (FESEM) technology (ZEISS Company). Surface characteristics were

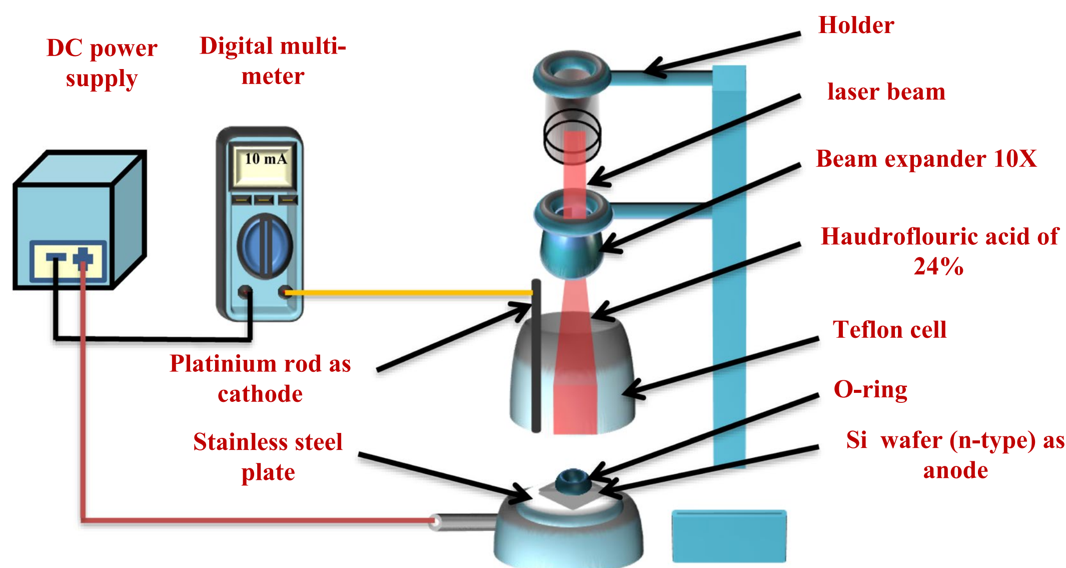

Figure 1. A schematic showing how a diode laser can aid the photo-electrochemical etching process[52].

assessed using atomic force microscopy (AFM) equipment from the TT-2 Workshop Company in the United States. Spectroscopic features were analyzed using photoluminescence (PL) techniques from the Perkin Elmer Company in the United States of America.

Preparation of gallium nitride pellet

A high-purity gallium nitride powder of 99.9%, purchased from Luoyang Advanced Material Company, was compressed into a pellet using a hydraulic compressor with a force of 10 tons. The GaN pellet was subjected to ablation using a Q-switching Nd:YAG laser (RY 280, China) with varying fluences ranging from 530 to 884 mJ/mm^2. The laser had a wavelength of 355 nm and a pulse duration of 7 ns, and the ablation process was conducted under a vacuum pressure of 10^{-2} mbar. The deposition of the GaN film onto the PSi substrate occurred at room temperature. The structure of the GaN film deposited on PSi was examined using an X-ray diffractometer (XRD6000, Shimadzu Company). The morphology of the deposited films was studied using field emission scanning electron microscopy (FESEM) from ZEISS Company. The topography of the deposited films was investigated using an atomic force microscope. Furthermore, the photoluminescence (PL) properties of the films were analyzed using a spectrophotometer from Perkin Elmer.

Electrical properties of GaN/PSi

To measure the electrical properties of the GaN/PSi photodetector, a metal interdigitated mask was employed for establishing ohmic contacts. An aluminum film was deposited onto the GaN layer and the backside of the silicon substrate using the thermal evaporation technique, as depicted in Fig. 2. The current–voltage characteristics of the photodetector were measured at room temperature under both dark and illuminated conditions. This was achieved using a power supply (Dazheng 30 V, 5 A PS-305D from China) and digital multi-meters (UNI-T UT33C). Additionally, a programmable LCR meter (LCR-6100, Taiwan, GW Instek, 10 Hz–100 kHz) was employed to evaluate the capacitance–voltage characteristics of the photodetector.

Figures of merit of the photodetector

The main figures of merit of the photodetector, namely responsivity (R), specific detectivity (D*), and external quantum efficiency (EQE) were measured using photodetector evaluation system. It is consists of monochromator

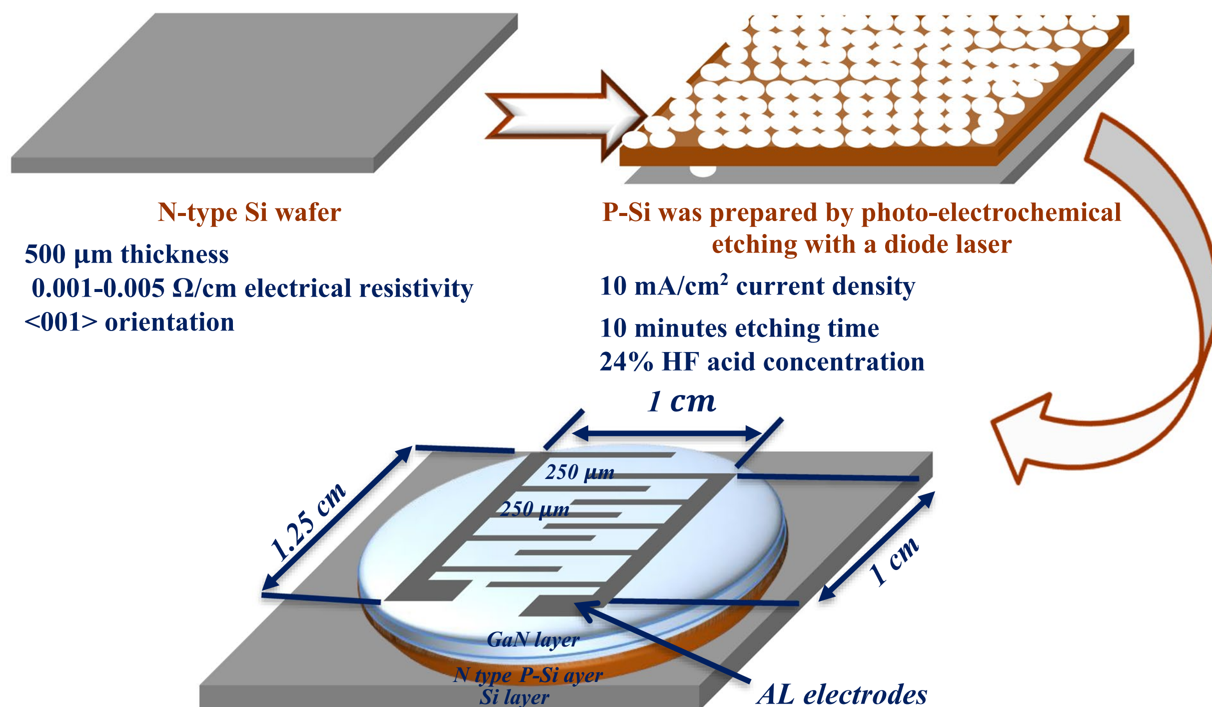

Figure 2. Process diagram of grown GaN nanostructure.

(Jobin-Yuvon), beam spilter, halogen lamp, multimeter, and silicon power meter. These measurements were conducted out under a reverse bias of 3 V.

Results and discussion

XRD properties

Figure 3 depicts the XRD pattern of the PSi, revealing two peaks situated at 2θ = 33° and 68°, which correspond to the (200) and (400) planes, respectively. These two peaks are characteristic of porous silicon and align well with findings reported previously[61–66]. The XRD analysis of PSi confirms the splitting of the peak at 68° into two distinct peaks, representing crystalline silicon and porous silicon..

Figure 4 depicts the XRD pattern of GaN nanocrystalline films deposited on PSi at various laser fluences. Three peaks were observed for all GaN films; these peaks are located at 2θ = 32.8°, 57.9°, and 61.7°, corresponding to (100), (110), and (103) planes, respectively. These peaks are indexed to GaN according to JCPDS # 01-074-0243. With an increase in laser fluence, a slight shift in 2θ was detected, and there was an observed increase in peak intensity along the (100) plane. The slight shift is attributed to stress and strain, while the increase in peak intensity is attributed to the greater film thickness and grain size.

The XRD analysis of the PSi substrate and the GaN films deposited on PSi is presented in Tables 1 and 2, respectively. To determine the crystallite size (D), Scherrer's formula[67–70] was employed, while the interplanar distance (d) was calculated using the formula[71–74]

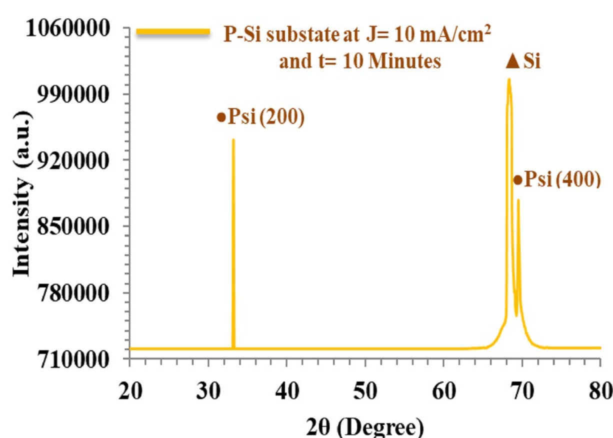

Figure 3. XRD pattern of PSi substrate.

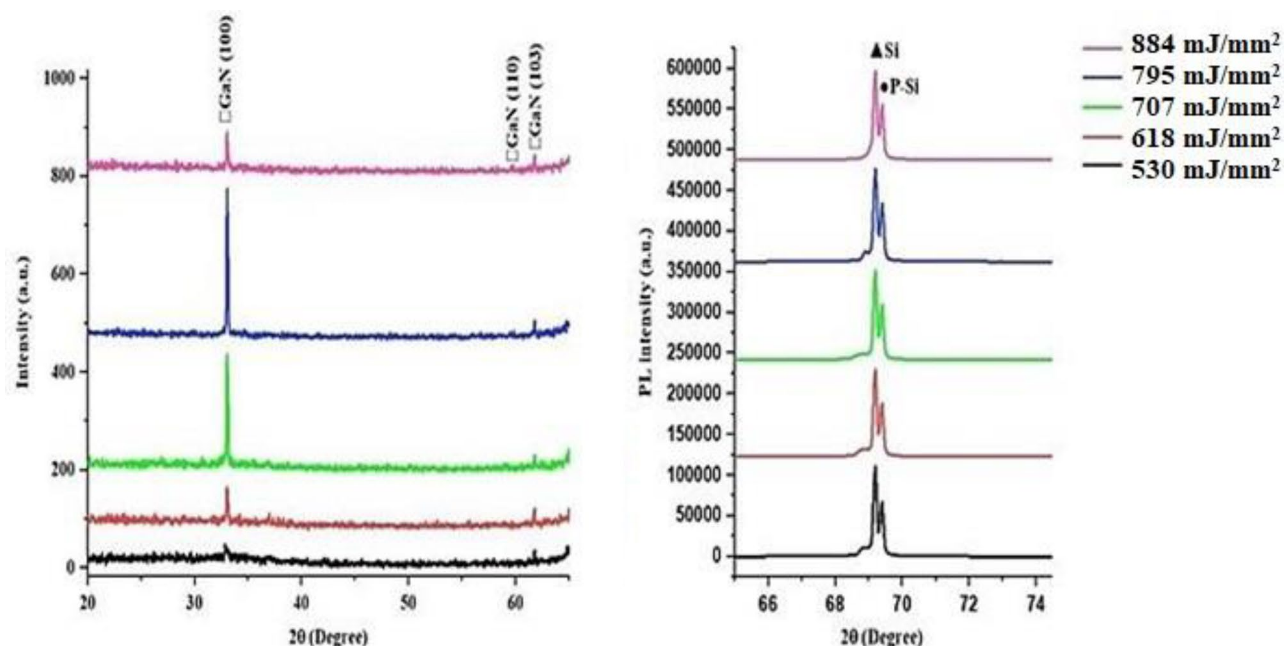

Figure 4. XRD pattern of GaN nano-crystalline films on a P-Si substrate using laser fluences ranging from 530 to 884 J.

Substrate orientation (hkl)	2 theta (Degree)	Full width at half maximum (Degree)	Crystallite size (nm)	Interplanner spacing (nm)
<200>	33.101	0.290	0.282	0.211
<400>	69.331	0.321	0.141	0.142

Table 1. X-Ray diffraction pattern of fabricated P-Si layer.

Laser Fluence (mJ/mm²)	Film orientation (hkl)	2theta (Degree)	Full width at half maximum (Degree)	Crystallite size (nm)	Interplanner spacing (nm)
530	<100>	32.840	0.390	21.260	0.271
	<110>	57.921	0.170	53.471	0.152
	<103>	61.720	0.170	54.501	0.151
618	<100>	33.0	0.202	40.861	0.271
	<110>	58.921	0.150	60.900	0.152
	<103>	61.761	0.141	66.202	0.151
707	<100>	33.041	0.181	46.090	0.271
	<110>	59.160	0.230	39.762	0.152
	<103>	61.761	0.161	57.922	0.151
795	<100>	33.041	0.170	48.801	0.271
	<110>	59.801	0.061	152.932	0.152
	<103>	61.760	0.130	71.291	0.151
884	<100>	33.041	0.171	48.802	0.271
	<110>	59.761	0.050	183.481	0.152
	<103>	61.760	0.131	71.292	0.151

Table 2. XRD pattern of GaN nano-crystalline films over P-Si substrate.

$$D = K\lambda/\beta \cos\theta \quad (2)$$

$$d = n\lambda/2 \sin\theta \quad (3)$$

where K is a constant set at 0.9, λ is the wavelength of the CuKα source, β is the fullwidth at half maximum of the XRD pattern,θ is the diffraction angle, and n is a positive integer.

Spectroscopic properties

The photoluminescence (PL) spectra of the PSi substrate are depicted in Fig. 5. PL measurements of the PSi substrate were conducted at room temperature with an excitation wavelength of 280 nm. Firstly, it is observed that the prepared PSi substrate exhibits an emission peak at 589 nm, which belongs to the visible yellow band. This peak is attributed to surface states and quantum confinement arising during the photo-electrochemical etching process, as mentioned by Wang[75–78]. The energy band gap of the prepared PSi substrate was determined to be 2.1 eV, larger than the energy band gap of crystalline silicon (1.11 eV). This difference in energy band gaps can be attributed to the combined effects of quantum confinement and increased surface states, altering the electronic structure of the material.

The PL spectra of GaN nanocrystalline films prepared at different laser fluences are depicted in Fig. 6. The PL of GaN/P-Si nanocrystalline films was measured at room temperature, and the excitation wavelength was 320 nm. The PL spectra of the GaN nanocrystalline films exhibited UV bands located at 265.9, 267.9, 267, 260, and 260.9 nm, which are attributed to the GaN film, as well as red bands at 628.9, 621, 625.9, 624, and 625 nm, which belong to the P-Si substrate. Increasing the laser fluence led to a decrease in the PL intensity, but there were differing opinions regarding the peak location of the PL spectrum. This discrepancy was likely due to the higher defect density causing more non-radiative recombination. According to the PL results, the energy gaps for GaN nanofilms prepared at laser fluences of 530, 618, 707, 884, and 795 mJ/mm^2 are 3.45, 3.38, 3.36, 3.34, and 3.44 eV, respectively, which are in agreement with the reported data[58,79–81].

Surface topography AFM

Figure 7 a,b depicts the 3D AFM images and the grain size distribution of P-Si substrate etched. In contrast, after 10 min of etching, the pores formed uniformly throughout the entire surface, taking on a more elongated oval shape. Table 3 provides the AFM parameters of a prepared P-Si substrate. Most notably, nanometer-scale research into particle size distribution was conducted on the P-Si substrate after preparation.

To analyze and characterize the topography of the prepared GaN nano-crystalline films over a PSi substrate, Fig. 8 depicts three-dimensional AFM images and grain size distribution. Average particle diameter and average

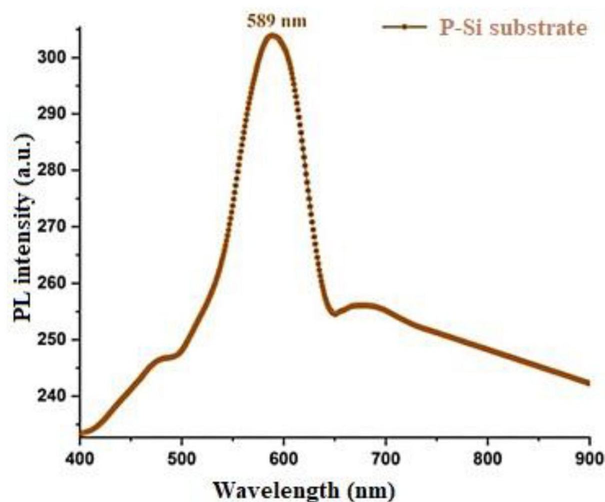

Figure 5. Room temperature photoluminescence prepared P-Si substrate.

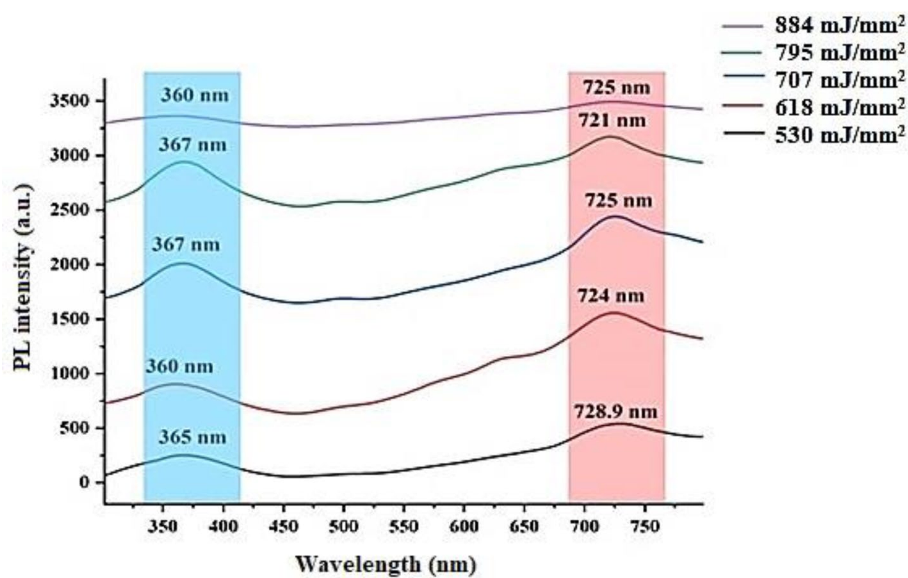

Figure 6. Room temperature PL spectra of GaN/PSi nanostructures prepared at various laser fluences.

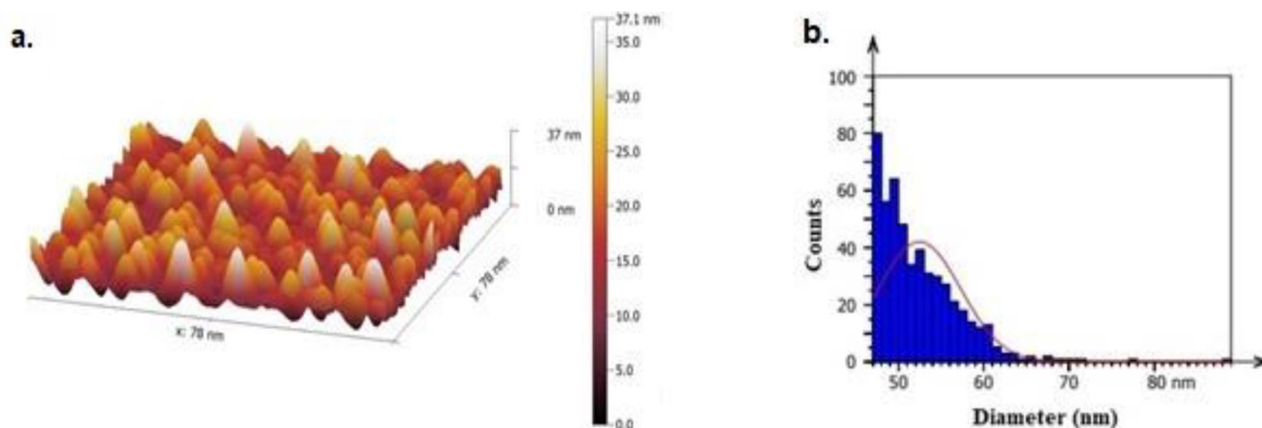

Figure 7. (**a**) AFM image of prepared P-Si substrate; (**b**) grain size distribution of prepared P-Si substrate.

Root-mean-square height (nm)	Maximum height (nm)	Average surface roughness (nm)	Average diameter (nm)
11.880	88.660	9.400	52.460

Table 3. AFM parameters of PSi substrate.

surface roughness increased as laser Fluence increased from 530 to 884 mJ/mm^2, but they decreased at 884 mJ/mm^2, as demonstrated in Table 4. The AFM image of the GaN nanocrystalline film shows the uniform deposition of samples created with 795 mJ/mm^2 laser Fluence and the largest average particle diameter and average surface roughness.

Surface morphology FESEM

Figure 9a and b depicts FE-SEM images of the surface and cross-section, respectively, of the PSi substrates, offering insights into the surface morphology. According to the research conducted by Omar et al.[67], the pores on the surface exhibit a star-like appearance and maintain an elongated shape across the entire surface. This is attributed to the use of n-type silicon (100) with low resistivity during the preparation of the PSi[82–85]. Furthermore, the FE-SEM cross-sectional image revealed that the thickness of the P-Si layer measures 36.02 µm.

Figure 10 depicts FE-SEM images of GaN/PSi nanostructures produced using PLD at varying laser intensities. This study revealed that the thickness of the GaN nanocrystalline film produced with a laser fluence of 795 mJ/mm^2 during the PLD process measures approximately 383.36 nm, which is comparable to the thickness of the GaN nanostructures themselves. The surface morphology of the GaN films was analyzed using micro- and nano-scale techniques. As depicted in Fig. 11, the average diameter of GaN/PSi nanostructures created with different laser fluences was calculated through ImageJ analysis. Furthermore, the GaN nano-crystalline films fully covered the P-Si substrate, resulting in uniform and homogeneously-sized spherical particles with a cauliflower-like shape.

Electrical properties

At room temperature, the dark current–voltage characteristic of the prepared P-Si substrate was analyzed in the dark, as depicted in Fig. 12A. As the voltage was applied, the current flowing through the P-Si substrate increased due to the elevated resistance of the P-Si layer with increasing voltage[86,87]. Moreover, the charge transfer led to the formation of a depletion zone in the prepared P-Si substrate close to the electrical dipole, resulting in a rectifying characteristic[88–90].

Figure 12B depicts the capacitance–voltage characteristic for applied voltages ranging from 0 to 3 V. The capacitance of the prepared P-Si substrate decreased. This phenomenon has been coined as the "growing depletion region with increasing built-in potential"[57,91–94].was coined to describe this phenomenon.

The relationship between 1/C^2 and the voltage on the fabricated P-Si substrate is depicted in Fig. 12C. C^2 exhibits a linear relationship with voltage. Figure 12C shows the correlation between 1/C^2 and voltage on a prepared PSi substrate. a linear relationship with voltage. The built-in potential was determined by extending the given linear segment of the curve to a 1/C^2 value of 0 points. There was an inherent potential of 0.34 eV.

Figure 13 depicts the dark I–V characteristics of GaN nanocrystalline films fabricated on a P-Si substrate using the PLD method at various laser fluences and at room temperature. As the bias voltage was increased, the GaN nano-crystalline film created at 795 mJ/mm^2 exhibited expansion due to the narrowing of the depletion layer[95,96].

Furthermore, rectification features were observed in the GaN/P-Si nanocrystalline film, and recombination tunneling served as the current transport mechanism in both layers[97–99].

Performance characterization of GaN nanostructure with optimum laser fluence

The performance properties of the fabricated GaN/PSi heterojunction using the PLD method with optimal laser parameters (355 nm laser wavelength and 300 °C substrate temperature) at different laser fluences were determined, and they are illustrated in Figs. 15, 16, 17 and 18. The study concluded that a laser Fluence value of 795 mJ/mm^2 was optimal. The responsivity (R_λ), specific detectivity (D_λ), and external quantum efficiency (EQE) of the produced GaN nano-crystalline film were assessed. Responsivity (R_λ) can be calculated using Eq. (4)[57,96,100,101], which stands as a significant figure of merit. Both Eqs. (5) and (6)[102–105] represent detectivity (D*) and external quantum efficiency (EQE), respectively

$$R_\lambda = \frac{I_{ph}}{P} \tag{4}$$

I_{ph} is the photocurrent (Ampere), and P is the incident power (Watt)[106,107].

$$D^*_\lambda = \frac{R_\lambda A^{1/2}}{\sqrt{2qI_{dark}}} \tag{5}$$

where A is the area of photodetector, I_{dark} is the dark current of photodetector, and q is the electron charge[108–111].

$$EQE = \frac{1240\ R_\lambda}{\lambda_{nm}} \tag{6}$$

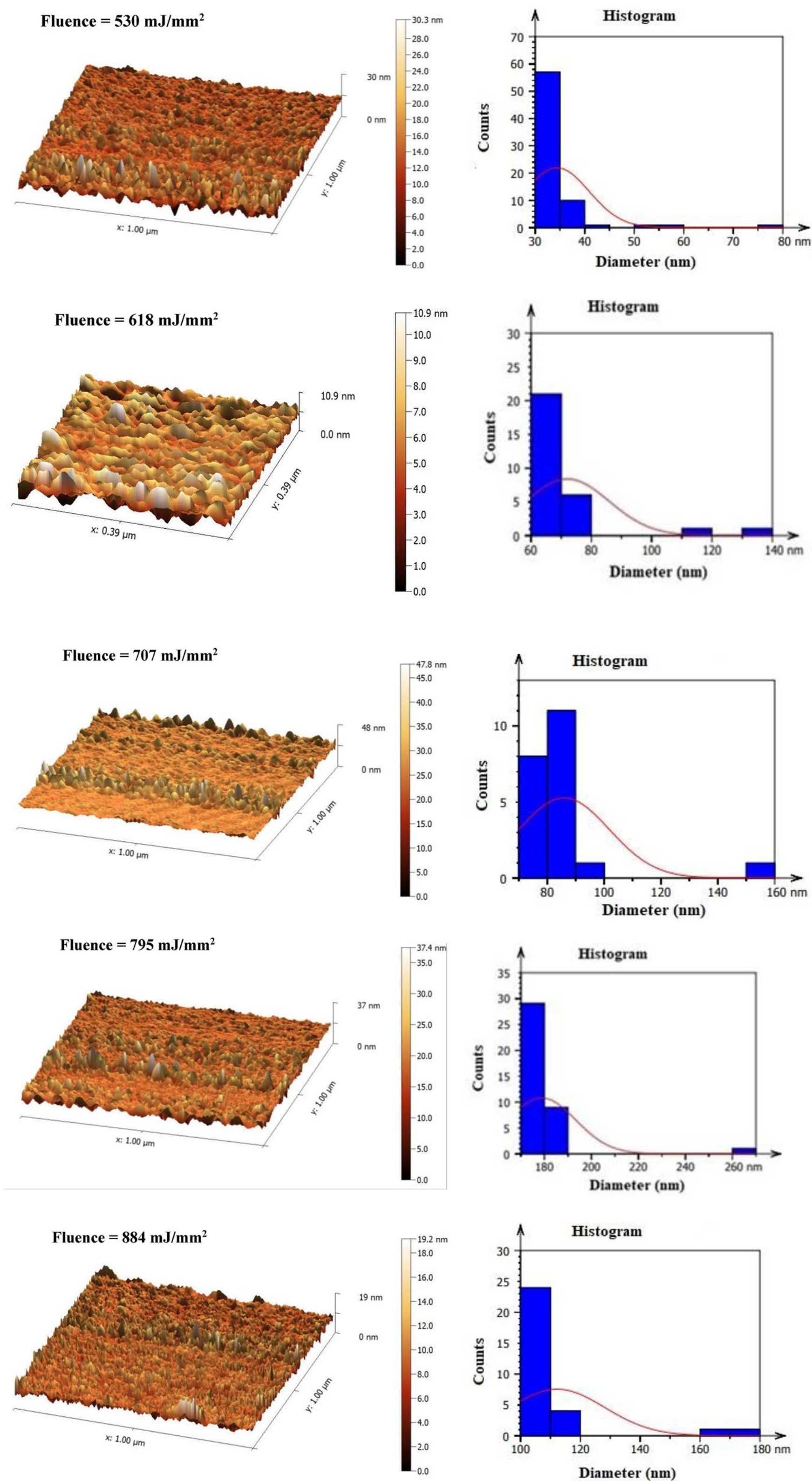

Figure 8. AFM and grain size distribution images of GaN/PSi nanostructures prepared at various laser fluences.

Laser fluence (mJ/mm^2)	Root-mean-square height (nm)	Maximum height (nm)	Average surface roughness (nm)	Average diameter (nm)
530	15.962	78.011	13.832	34.411
618	34.411	131.701	28.423	72.051
707	46.822	154.321	42.521	85.932
795	59.012	265.301	50.610	178.83
884	33.853	179.702	26.012	112.222

Table 4. AFM parameters of GaN/PSi nanostructures prepared at various laser fluences.

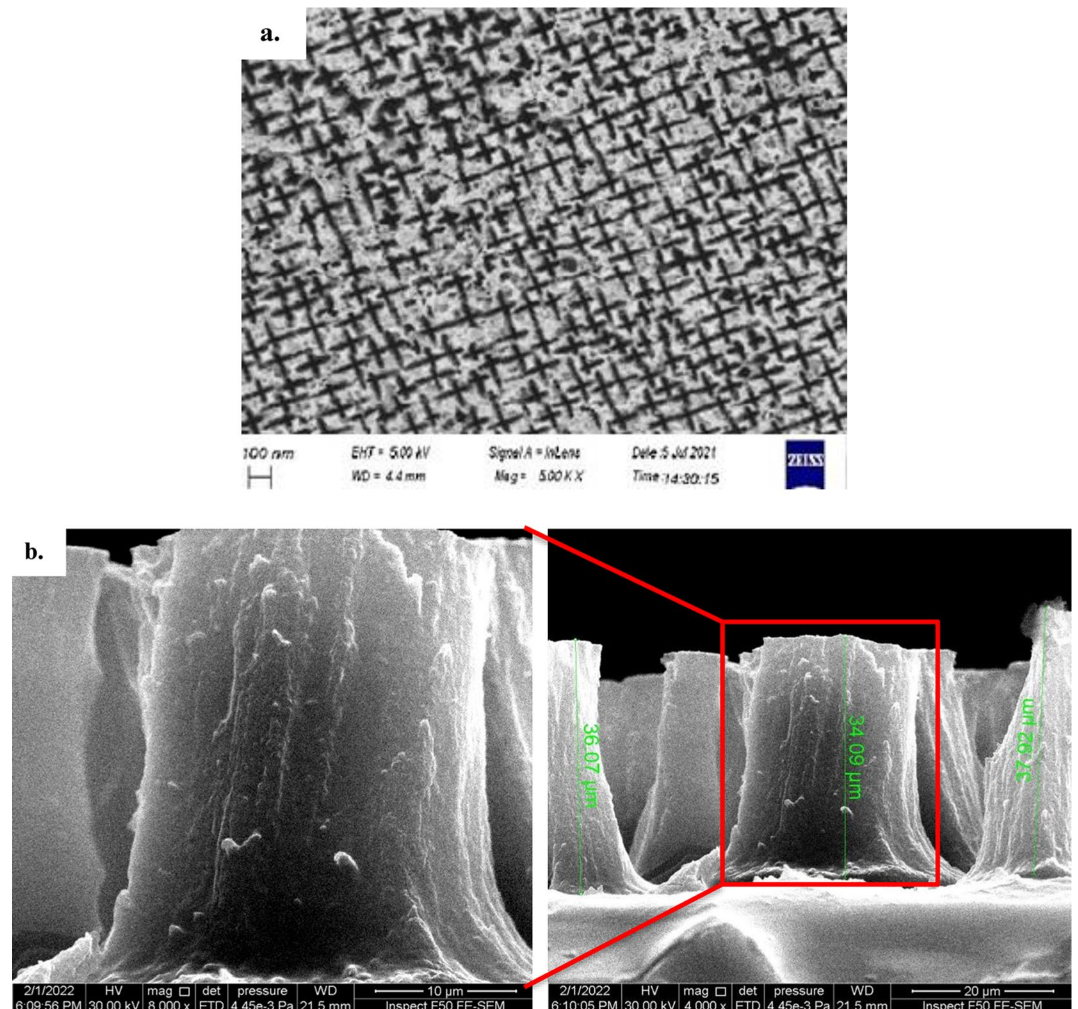

Figure 9. FE-SEM images of prepared P-Si substrate, a. surface area image, and b. cross section image.

Figure 14 depicts the responsivity of the structure when subjected to varying laser intensities operating between 350 and 850 nm. Three response peaks of 29.010 A/W at 370 nm and 22.761 A/W at 550 nm were observed in the fabricated GaN on P-Si nanostructure at 795 mJ/mm^2, which can be attributed to the larger surface area, extended depletion layer width, and increased minority carrier diffusion length[112].

Figure 15 depicts variation of detectivity (D*) with wavelength of the GaN/P-Si photodetectors. Two peaks were observed at 355 nm and 550 nm.

Figure 16 depicts the EQE of GaN/PSi photodetectors fabricated at various laser fluences. Among these, the photodetector fabricated at 795 mJ/mm^2 achieved the highest EQE values: 93.240% at 370 nm and 51.30% at 550 nm. The GaN/PSi heterojunction photodetector fabricated at 795 mJ/mm^2 demonstrated a high EQE due to the direct relationship with Eq. (6), driven by its strong spectral response. Enhancing the reverse bias voltage can improve the collection efficiency of photogenerated carriers, allowing for the creation of a fully depleted photodetector[113,114].

Figures 17 and 18 depict the dynamic photoresponse switching of the photodetectors deposited at various laser fluences. Three distinct switching cycles were conducted, each with an 18-s off period followed by a 25-s

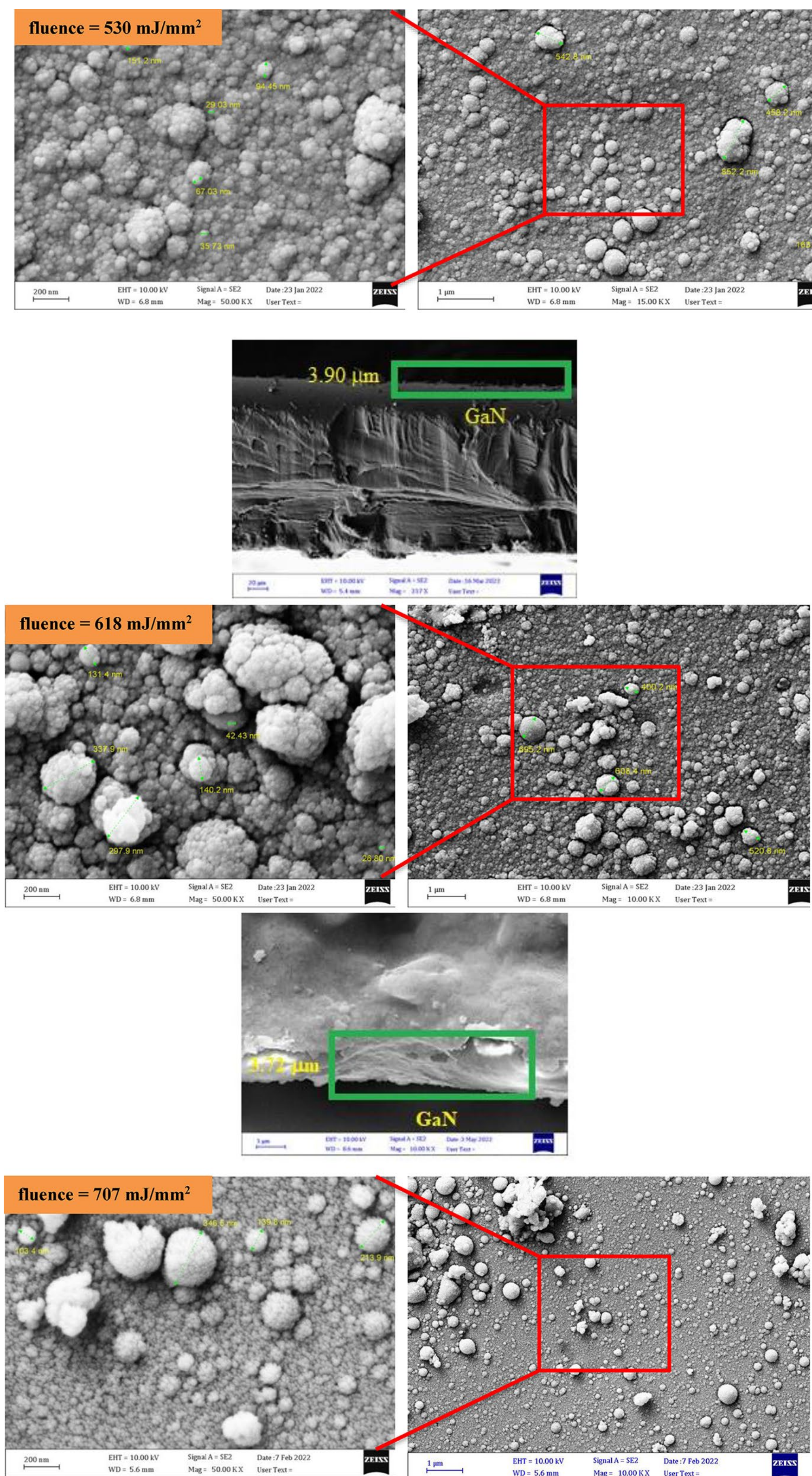

Figure 10. FE-SEM images and cross section images of GaN/PSi nanostructures prepared at various laser fluences.

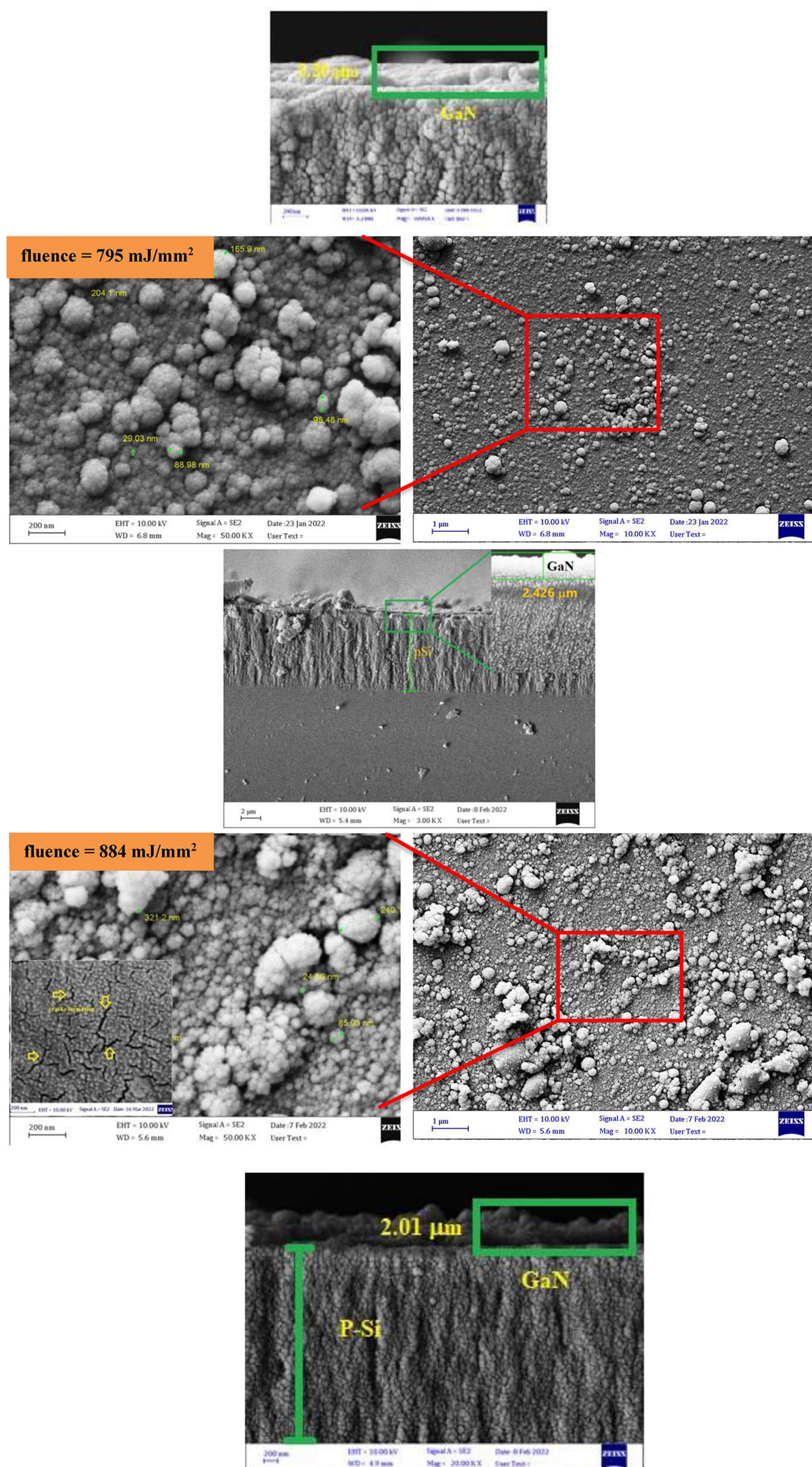

Figure 10. (continued)

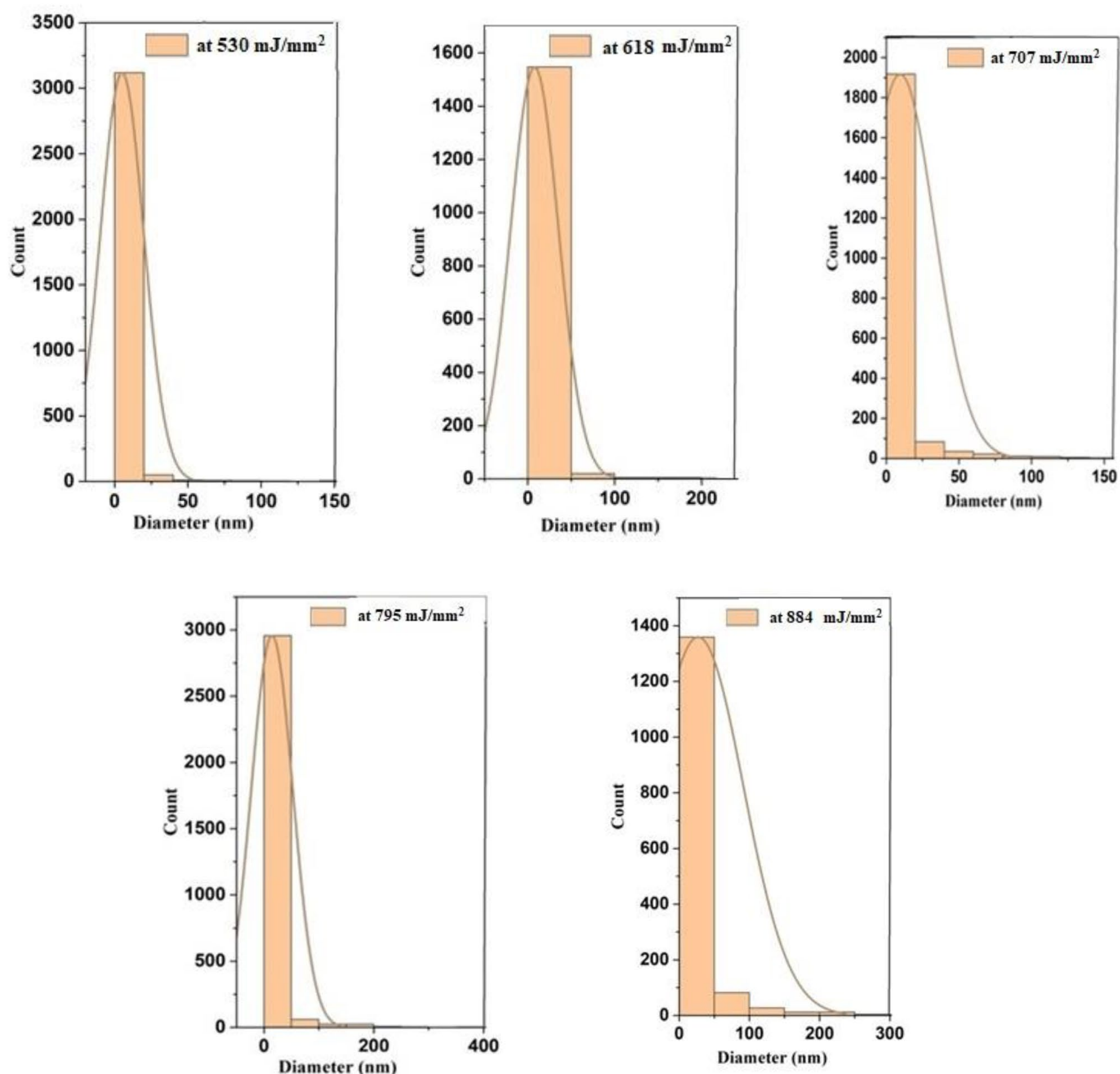

Figure 11. Average diameter images of GaN/PSi nanostructures prepared at various laser fluences.

on period. Rise and fall times of the fabricated GaN/P-Si nanostructure were measured from 10 to 90% of the peak signal and from 90 to 10% of the peak signal, respectively. The photodetector prepared with a laser fluence of 795 mJ/mm^2 exhibits a switching characteristic, with a measured rise time of 363 µs and a fall time of 711 µs.

The fabricated GaN/P-Si nanocrystalline film at 795 mJ/mm^2 exhibited the best performance, with a responsivity of 29.010 A/W at 370 nm, a detectivity of 8.61×10^{12} Jones, and an external quantum efficiency of 93.240%. Additionally, it demonstrated a fast response rise time of 328 and a fall time of 617, outperforming Jiang et al. (2022), who fabricated a GaN/Si UV photodetector using a chemical vapor deposition process. Their device showed a responsivity of 71.4 mA/W, detectivity of 7.1×10^{8} Jones, external quantum efficiency of 24.3%, and a response time of 0.2/7.6 s[115]. Table 5 provides a summary of the figures of merit for the GaN/PSi photodetectors fabricated at various laser fluences.

Conclusion

Nanostructured GaN/PSi photodetectors were successfully fabricated using the pulsed laser deposition method at various laser fluences. The GaN nanostructure film deposited at 795 mJ/mm^2 exhibited high crystalline peaks with a large crystallite size, indicating favorable structural characteristics. Spectroscopically, this film exhibited a shorter wavelength of 260 nm and a high energy gap of 4.76 eV. Morphologically, the film showed uniform,

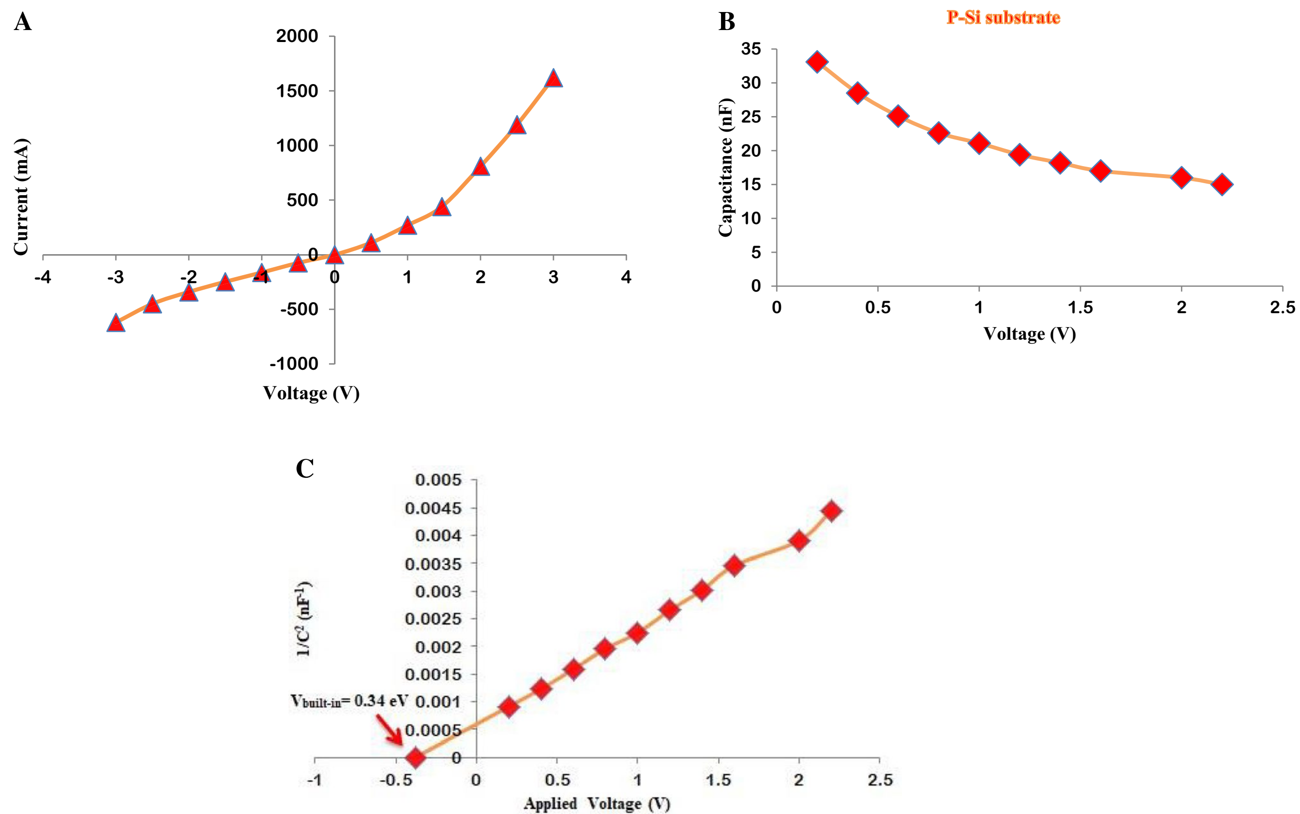

Figure 12. Electrical characteristic of prepared P-Si substrate, (**A**) dark I–V characteristic for forward and reverse bias, (**B**) C–V characteristic, (**C**) $1/C^2$ vs. voltage.

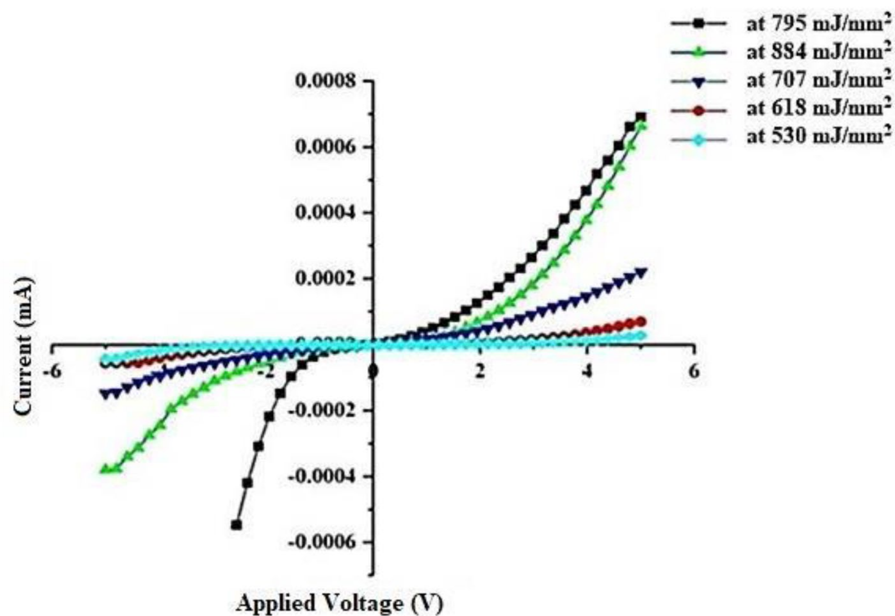

Figure 13. PLD-fabricated GaN/PSi nanostructure dark I–V properties at laser fluences between 530 and 884 mJ/mm^2 under forward and reverse biases.

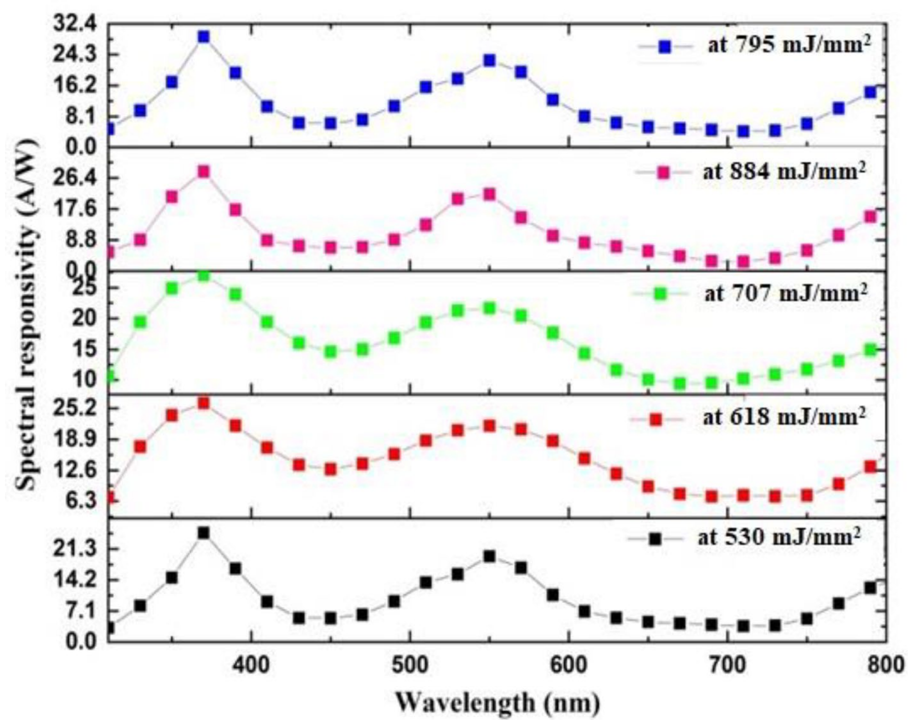

Figure 14. Spectral responsivityof fabricated GaN/P-Si nanostructure at 355 nm, 300 °C and different laser fluences.

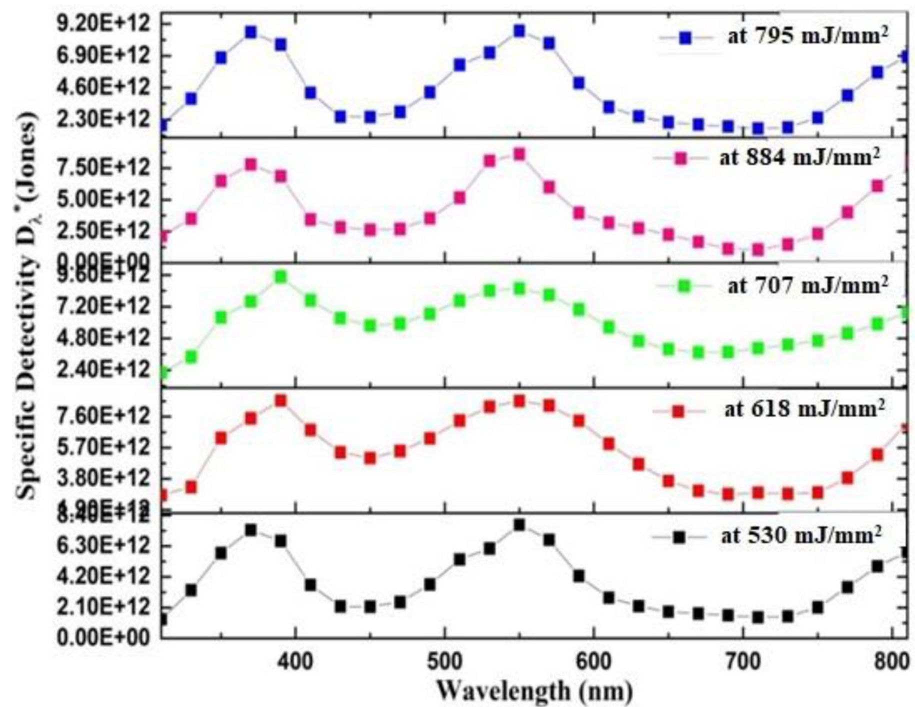

Figure 15. Detectivity of GaN/P-Si heterojunction photodetectors fabricated at different laser fluences under − 3 V bias.

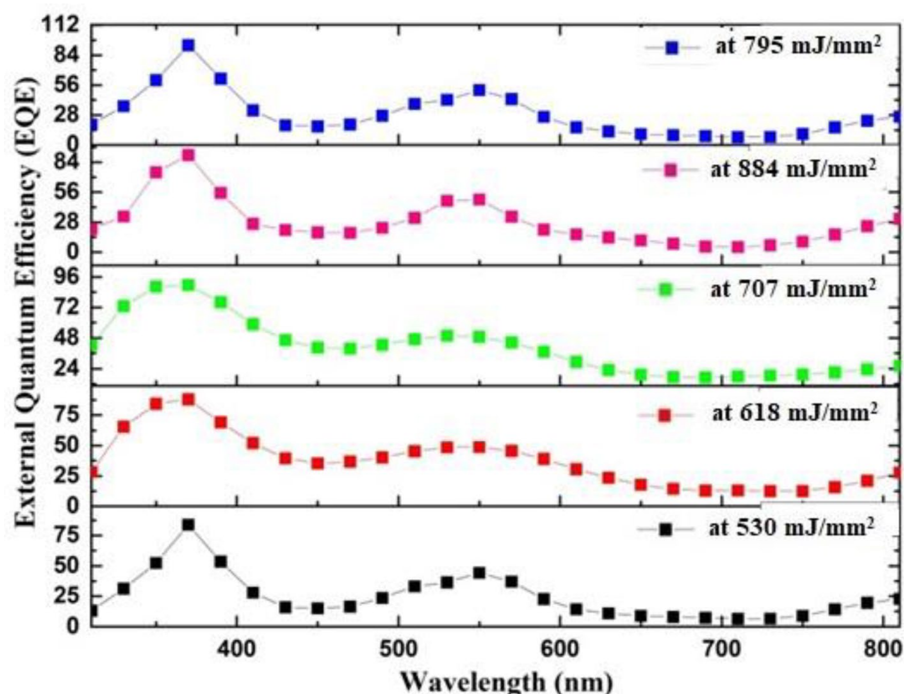

Figure 16. External quantum efficiency of GaN/P-Si nanostructure fabricated at different laser fluences.

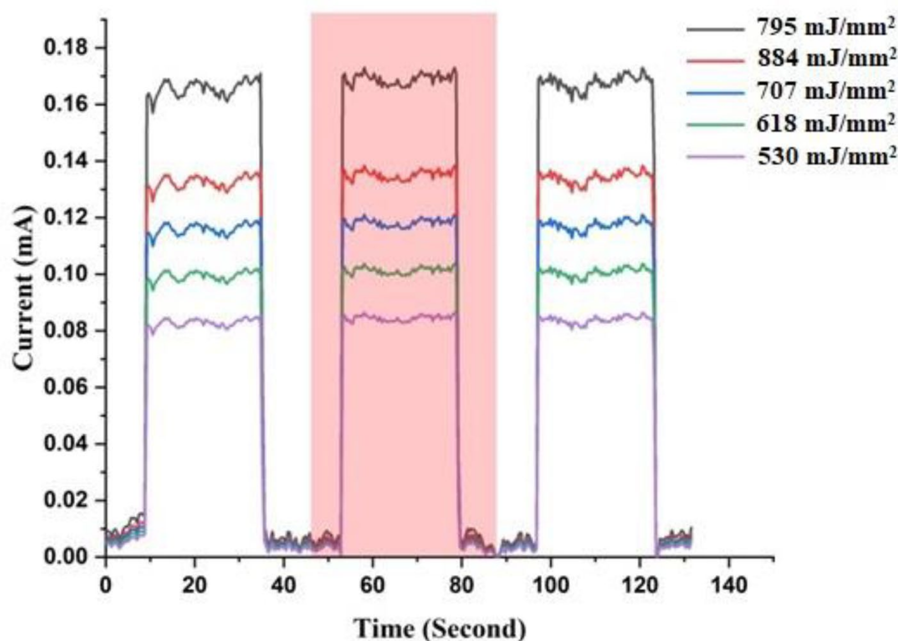

Figure 17. A switching characteristic of GaN/P-Si nanostructure fabricated at different laser fluences.

homogeneous spherical particles resembling cauliflower, with a thickness of 383.36 nm. Additionally, a uniform deposition yielded the largest average particle diameter (178.8 nm) and average surface roughness (50.61 nm).

Furthermore, performance characteristics were assessed for GaN nanostructures prepared using a laser fluence of 795 mJ/mm^2. Due to the energy gap of GaN material, the responsivity under 3 V exhibited maximum values: responsivity of approximately 29.03 A/W, detectivity of 8.6×10^{12} Jones, and an external quantum efficiency of 97.2% at 370 nm. Similarly, at 575 nm, the responsivity measured around 19.86 A/W, detectivity of 8.9×10^{12} Jones, and an external quantum efficiency of 50.89%.

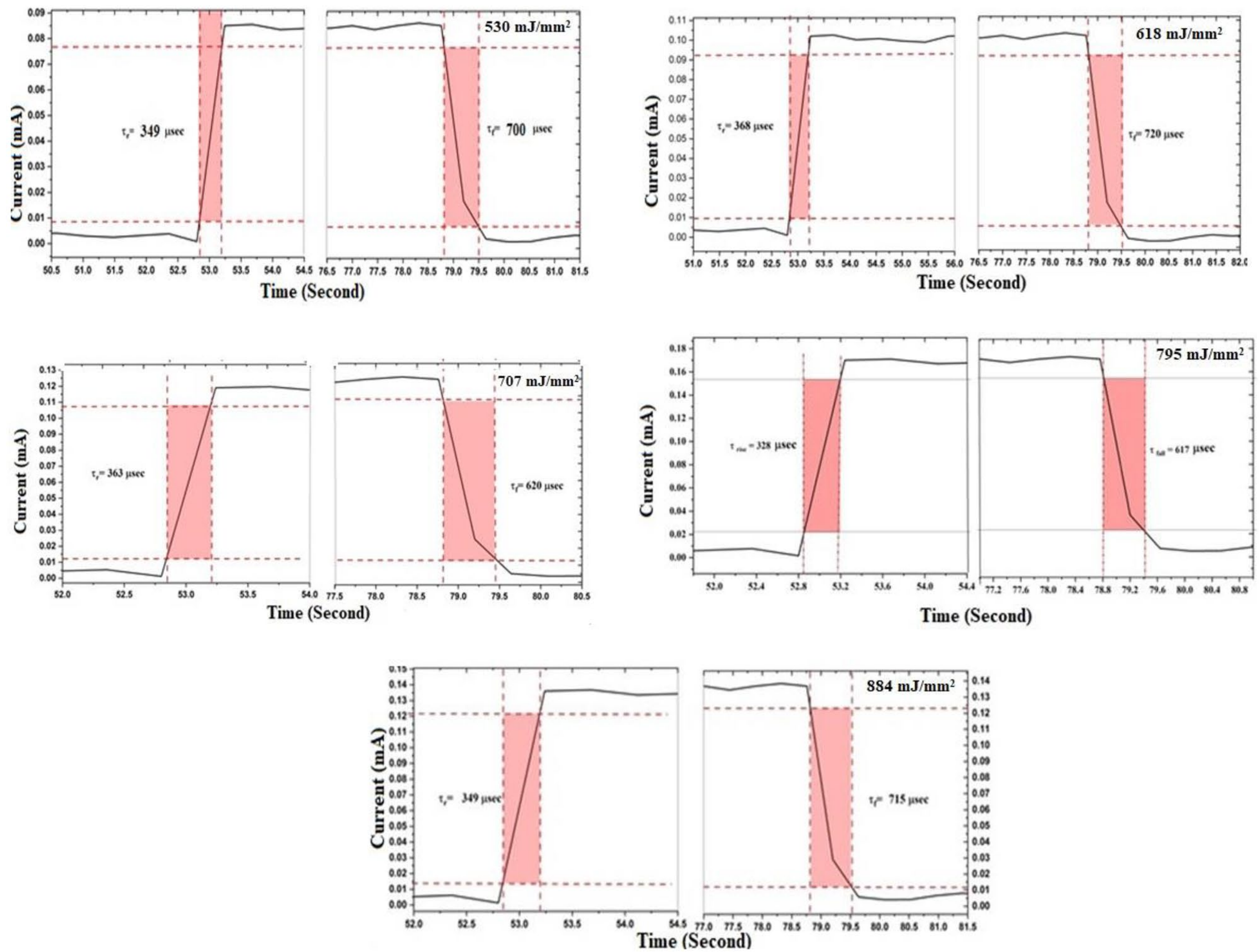

Figure 18. Rise time and fall time of GaN/PSi heterojunction photodiode fabricated at different laser fluences.

Laser fluence (mJ/mm^2)	Spectral responsivity (A/W)	Specific detectivity (Jones)	External quantum efficiency (%)	Rise time (μs)	Fall time (μs)
530	25.011 at 370 nm	$7.40 \times 10^{+12}$	83.801	349	700
	19.620 at 550 nm	$7.750 \times 10^{+12}$	44.212		
618	26.271 at 370 nm	$7.51 \times 10^{+12}$	88.051	368	720
	21.660 at 575 nm	$8.51 \times 10^{+12}$	48.812		
707	27.081 at 370 nm	$7.60 \times 10^{+12}$	89.512	363	620
	21.701 at 555 nm	$8.50 \times 10^{+12}$	48.911		
795	29.010 at 370 nm	$8.61 \times 10^{+12}$	93.240	328	617
	22.762 at 555 nm	$8.70 \times 10^{+12}$	51.306		
884	28.192 at 370 nm	$7.81 \times 10^{+12}$	90.702	349	715
	21.811 at 555 nm	$8.60 \times 10^{+12}$	49.110		

Table 5. Shows the results of testing a manufactured GaN/P-Si nanostructure fabricated at different laser fluences.

Additionally, three switching cycles with an 18-s off period and a 25-s on period were illuminated with a power of 100 mW/cm^2. The rise time of the fabricated GaN/P-Si nanostructure was 328 µs, while the fall time was 617 µs. A strong correlation was observed between the optimum laser Fluence (795 mJ/mm^2) and the achieved GaN nanostructure performance characteristics.

Data availability

Correspondence and requests for materials should be addressed to Makram A. Fakhri, Haneen D. Jabbar, and Evan T. Salim.

Received: 18 September 2023; Accepted: 20 November 2023
Published online: 29 November 2023

References

1. Chen, F., Ji, X. & Lau, S. P. Recent progress in group III-nitride nanostructures: From materials to applications. *Mater. Sci. Eng. R. Rep.* **142**, 100578 (2020).
2. Feng, Z. C. (ed.) *III-Nitride Materials* (World Scientific, 2017).
3. Gil, B. *III-Nitride Semiconductors and Their Modern Devices* (OUP Oxford, 2013).
4. Kneissl, M. & Rass, J. *III-Nitride Ultraviolet Emitters* (Springer, 2016).
5. Ben, J. *et al.* 2D III-Nitride materials: Properties, growth, and applications. *Adv. Mater.* **33**(27), 2006761 (2021).
6. Flack, T. J., Pushpakaran, B. N. & Bayne, S. B. GaN technology for power electronic applications: A review. *J. Electron. Mater.* **45**(6), 2673–2682 (2016).
7. Boles, T. (GaN-on-silicon present challenges and future opportunities. In *2017 12th European Microwave Integrated Circuits Conference (EuMIC)* 21–24 (IEEE, 2017).
8. Amir, H. A. A. A. *et al.* Synthesis of gallium nitride nanostructure using pulsed laser ablation in liquid for photoelectric detector. *Mater. Sci. Semicond. Process.* **150**, 106911 (2022).
9. Abud, S. H., Selman, A. M. & Hassan, Z. Investigation of structural and optical properties of GaN on flat and porous silicon. *Superlattices Microstruct.* **97**, 586–590 (2016).
10. Jabbar, H. D., Fakhri, M. A. & AbdulRazzaq, M. J. Gallium nitride-based photodiode: A review. *Mater. Today: Proc.* **42**, 2829–2834 (2021).
11. Roccaforte, F., Fiorenza, P., Lo Nigro, R., Giannazzo, F. & Greco, G. Physics and technology of gallium nitride materials for power electronics. *La Riv. Nuovo Cimen.* **41**(12), 625–681 (2018).
12. Al-Zuhairi, O. *et al.* Non-polar gallium nitride for photodetection applications: A systematic review. *Coatings* **12**(2), 275 (2022).
13. Amir, H. A. A. A., Fakhri, M. A., Alwahib, A. A. & Salim, E. T. Synthesize of GaN/quartz nanostructure using pulsed laser ablation in liquid for optoelectronic devices. *Sens. Actuat. B: Chem.* **2021**, 2163 (2021).
14. Amir, H. A. A. A. *et al.* An investigation on GaN/Porous-Si NO2 gas sensor fabricated by pulsed laser ablation in liquid. *Sens. Actuat. B: Chem.* **2022**, 132163 (2022).
15. Aggarwal, N. & Gupta, G. Enlightening gallium nitride-based UV photodetectors. *J. Mater. Chem. C* **8**(36), 12348–12354 (2020).
16. Xu, W. *et al.* Magnesium ion-implantation-based gallium nitride pin photodiode for visible-blind ultraviolet detection. *Photon. Res.* **7**(8), B48–B54 (2019).
17. Pham, T. T. T., Shin, H., Chong, E. & Cha, H. Y. Gallium nitride PIN avalanche photodiode with double-step mesa structure. *J. Semicond. Technol. Sci.* **18**(5), 645–649 (2018).
18. Yakuphanoglu, F. *et al.* A new type photodiode: p-Si/GaN pn junction in series with GaN/Ag Schottky diode. *J. Alloy. Compd.* **650**, 671–675 (2015).
19. Ji, M. H. *et al.* Uniform and reliable GaN pin ultraviolet avalanche photodiode arrays. *IEEE Photon. Technol. Lett.* **28**(19), 2015–2018 (2016).
20. Bakhtiary-Noodeh, M. *et al*. Demonstration of uniform 6x6 GaN pin UV avalanche photodiode arrays. In *Gallium Nitride Materials and Devices XVI, vol. 11686* 93–100 (SPIE, 2021).
21. Griffiths, A. D., Herrnsdorf, J., McKendry, J. J. D., Strain, M. J. & Dawson, M. D. Gallium nitride micro-light-emitting diode structured light sources for multi-modal optical wireless communications systems. *Philos. Trans. R. Soc. A* **378**(2169), 20190185 (2020).
22. Wang, Y. *et al.* A monolithically integrated gallium nitride nanowire/silicon solar cell photocathode for selective carbon dioxide reduction to methane. *Chem. Eur. J.* **22**(26), 8809–8813 (2016).
23. Zulkifli, N. A. A. *et al.* A highly sensitive, large area, and self-powered UV photodetector based on coalesced gallium nitride nanorods/graphene/silicon (111) heterostructure. *Appl. Phys. Lett.* **117**(19), 191103 (2020).
24. Li, G., Wang, W., Yang, W. & Wang, H. Epitaxial growth of group III-nitride films by pulsed laser deposition and their use in the development of LED devices. *Surf. Sci. Rep.* **70**(3), 380–423 (2015).
25. Wong, S. & Jaluria, Y. A numerical and experimental study on the fabrication GaN films by chemical vapor deposition. *J. Manuf. Sci. Eng.* **142**(1), 011001 (2020).
26. Wang, W., Wang, H., Yang, W., Zhu, Y. & Li, G. A new approach to epitaxially grow high-quality GaN films on Si substrates: The combination of MBE and PLD. *Sci. Rep.* **6**(1), 1–11 (2016).
27. Shetty, A. *et al*. (Plasmonic enhancement of photocurrent in GaN based UV photodetectors. In *2014 IEEE 2nd International Conference on Emerging Electronics (ICEE)* 1–4 (IEEE, 2014).
28. Salim, E. T., Hassan, A. I. & Naaes, S. A. Effect of gate dielectric thicknesses on MOS photodiode performance and electrical properties. *Mater. Res. Express* **6**(8), 086416 (2019).
29. Lin, J. C. *et al.* High responsivity of GaN p-i-n photodiode by using low-temperature interlayer. *Appl. Phys. Lett.* **91**(17), 173502 (2007).
30. ElFaham, M. M., Mostafa, A. M. & Toghan, A. Facile synthesis of Cu2O nanoparticles using pulsed laser ablation method for optoelectronic applications. *Colloids Surf. A* **630**, 127562 (2021).
31. Tareq, H. S. Deposited nanostructure cds thin film by using pulse laser deposition technique for fabrication of heterojunction solar cell. *Eng. Tech. J.* **32**, 141 (2014).
32. Abdulkareem, K. A., Kadhim, S. M. & Ali, S. B. The structural and optical properties of nanocrystalline Fe3O4 thin films prepared by PLD. *Eng. Technol. J.* **40**(02), 334–342 (2022).
33. Abdul Amir, H. A. A., Fakhri, M. A. & Alwahib, A. Synthesized of GaN nanostructure using 1064 nm laser wavelength by pulsed laser ablation in liquid. *Eng. Technol. J.* **40**(2), 404–411 (2022).
34. Taleb, S. M., Fakhri, M. A., & Adnan, S. A. Optical investigations of nanophotonic LiNbO3 films deposited by pulsed laser deposition method. In *Defect and Diffusion Forum, vol. 398* 16–22 (Trans Tech Publications Ltd, 2020).
35. Khalid, F. G., Ibraheam, A. S., Fakhri, M. A., & Numan, N. H. Some of the electrical and thermoelectrical properties for Cdo thin films preperaerd using pulsed laser deposition method. In *AIP Conference Proceedings, vol. 2213* 020204 (AIP Publishing LLC, 2020).
36. Fakhri, M. A. *et al.* Synthesis of LiNbO3/SiO2/Si nanostructures layer by layer based on mach-zehnder modulator using pulsed laser deposition route. *Silicon* **2022**, 1–15 (2022).
37. Chidambaram, P. R., Bowen, C., Chakravarthi, S., Machala, C. & Wise, R. Fundamentals of silicon material properties for successful exploitation of strain engineering in modern CMOS manufacturing. *IEEE Trans. Electron. Dev.* **53**(5), 944–964 (2006).
38. Basu, S. (Ed.). *Crystalline Silicon: Properties and Uses*. (BoD–Books on Demand, 2011).
39. Sun, P., Xu, P., Zhu, K., & Zhou, Z. Silicon-based optoelectronics enhanced by hybrid plasmon polaritons: Bridging dielectric photonics and nanoplasmonics. In *Photonics, vol. 8* 482. MDPI (2021).
40. Sharma, P., Sun, X., Parish, G. & Keating, A. Optimising porous silicon electrical properties for thermal sensing applications. *Micropor. Mesopor. Mater.* **312**, 110767 (2021).

41. Vercauteren, R., Scheen, G., Raskin, J. P. & Francis, L. A. Porous silicon membranes and their applications: Recent advances. *Sens. Actuat. A* **318**, 112486 (2021).
42. Jung, Y., Huh, Y. & Kim, D. Recent advances in surface engineering of porous silicon nanomaterials for biomedical applications. *Micropor. Mesopor. Mater.* **310**, 110673 (2021).
43. Moretta, R., De Stefano, L., Terracciano, M. & Rea, I. Porous silicon optical devices: Recent advances in biosensing applications. *Sensors* **21**(4), 1336 (2021).
44. Jenie, S. N., Plush, S. E. & Voelcker, N. H. Recent advances on luminescent enhancement-based porous silicon biosensors. *Pharmaceut. Res.* **33**(10), 2314–2336 (2016).
45. Congli, S. *et al.* Synthesis of porous silicon nano-wires and the emission of red luminescence. *Appl. Surface Sci.* **282**, 259–263 (2013).
46. Arshavsky-Graham, S., Massad-Ivanir, N., Segal, E. & Weiss, S. Porous silicon-based photonic biosensors: Current status and emerging applications. *Anal. Chem.* **91**(1), 441–467 (2018).
47. Canham, L. (ed.) *Handbook of Porous Silicon* 163–170 (Springer International Publishing, 2014).
48. Kim, D. H., Lee, W. & Myoung, J. M. Flexible multi-wavelength photodetector based on porous silicon nanowires. *Nanoscale* **10**(37), 17705–17711 (2018).
49. Ismail, R. A., Alwan, A. M. & Ahmed, A. S. Preparation and characteristics study of nano-porous silicon UV photodetector. *Appl. Nanosci.* **7**(1), 9–15 (2017).
50. Santos, H. A., Mäkilä, E., Airaksinen, A. J., Bimbo, L. M. & Hirvonen, J. Porous silicon nanoparticles for nanomedicine: Preparation and biomedical applications. *Nanomedicine* **9**(4), 535–554 (2014).
51. Jabbar, H. D. *et al.* Effect of different etching time on fabrication of an optoelectronic device based on GaN/Psi. *J. Renew. Mater.* **11**(3), 1101–1122 (2023).
52. Jabbar, H. D., Fakhri, M. A. & AbdulRazzaq, M. J. Synthesis gallium nitride on porous silicon nano-structure for optoelectronics devices. *Silicon* **2022**, 1–17 (2022).
53. Hattab, F. & Fakhry, M. Optical and structure properties for nano titanium oxide thin film prepared by PLD. In *2012 First National Conference for Engineering Sciences (FNCES 2012)*. https://doi.org/10.1109/NCES.2012.6740474.
54. Asady, H., Salim, E. T. & Ismail, R. A. Some critical issues on the structural properties of Nb2O5 nanostructure film deposited by hydrothermal technique. *AIP Conf. Proc.* **2213**(1), 020183 (2020).
55. Fakhri, M. A., Al-Douri, Y. & Hashim, U. Fabricated optical strip waveguide of nanophotonics lithium niobate. *IEEE Photon. J.* **8**(2), 4500410. https://doi.org/10.1109/JPHOT.2016.2531583 (2016).
56. Mohammed, F. A., Salim, E. T., Hassan, A. I. & Wahid, M. H. A. Effect of precursor concentration on the structural, optical, and electrical properties of WO3 thin films prepared by spray pyrolysis. *J. Appl. Sci. Nanotechnol.* **2**(4), 91–105 (2022).
57. Fakhri, M. A. *et al.* Responsivity and response time of nano silver oxide on silicon heterojunction detector. *Int. J. Nanoelectron. Mater.* **11**(21), 65–72 (2018).
58. Alwazny, M. S., Ismail, R. A. & Salim, E. T. Optical properties of lithium niobate nanoparticles prepared by laser ablation in different surfactant solutions. *J. Appl. Sci. Nanotechnol.* **3**(1), 42–50 (2023).
59. Mohammed, D. A., Kadhim, A. & Fakhri, M. A. The enhancement of the corrosion protection of 304 stainless steel using Al2O-3films by PLD method. *AIP Conf. Proc.* **2045**, 020014. https://doi.org/10.1063/1.5080827 (2018).
60. Ismail, R. A., Yehya, K. Z. & Abdulrazaq, O. A. Preparation and characterization of In_2O_3 thin films for optoelectronic applications. *Surface Rev. Lett.* **12**, 515–518 (2005).
61. Fakhri, M. A. *et al.* Fabrication of UV photodetector based on GaN/Psi heterojunction using pulse laser deposition method: Effect of different laser wavelengths. *Opt. Mater.* **137**, 113593 (2023).
62. Salim, E. T., Agool, I. R. & Muhsien, M. A. Construction of SnO2/SiO2/Si heterojunction and its lineup using I-V and C-V measurements. *Int. J. Modern Phys. B* **25**(29), 3863–3869 (2011).
63. Salim, S. H., Al-Anbari, R. H. & Haider, A. Polysulfone/TiO2 thin film nanocomposite for commercial ultrafiltration membranes. *J. Appl. Sci. Nanotechnol.* **2**(1), 80–89 (2022).
64. Abdulrazzaq, O. A. & Saleem, E. T. Inexpensive near-IR photodetector. *Turk. J. Phys.* **30**, 35–39 (2006).
65. Fakhri, M. A. *et al.* Structural properties and surface morphology analysis of nanophotonic LINBO3. *ARPN J. Eng. Appl. Sci.* **11**(8), 4974–4978 (2016).
66. Salim, E. T. Rapid thermal oxidation for silicon nanocrystal based solar cell. *Int. J. Nanoelectron. Mater.* **5**(2), 95–100 (2012).
67. Omar, K. & Salman, K. A. Effects of electrochemical etching time on the performance of porous silicon solar cells on crystalline n-type (100) and (111). *J. Nano Res.* **46**, 45–56 (2017).
68. Salim, E. T. Optoelectronic properties of Fe2O3/Si heterojunction prepared by rapid thermal oxidation method. *Indian J. Phys.* **87**(4), 349–353. https://doi.org/10.1007/s12648-012-0229-5 (2013).
69. Fakhri, M. A., Hashim, U., Salim, E. T. & Salim, Z. T. Preparation and charactrization of photonic LiNbO3generated from mixing of new raw materials using spry pyrolysis method. *J. Mater. Sci. Mater. Electron.* **27**(12), 13105–13112. https://doi.org/10.1007/s10854-016-5455-8 (2016).
70. Salim, E. T., Al-Wazny, M. S. & Fakhri, M. A. Glancing angle reactive pulsed laser deposition (GRPLD) for Bi 2O3/Si heterostructure. *Modern Phys. Lett. B* **27**(16), 1350122. https://doi.org/10.1142/S0217984913501224 (2013).
71. Kang, B. K. *et al.* Formation of highly efficient dye-sensitized solar cells by effective electron injection with GaN nanoparticles. *J. Electrochem. Soc.* **158**(7), H693 (2011).
72. Salim, E. T., Fakhri, M. A. & Hassen, H. Metal oxide nanoparticles suspension for optoelectronic devises fabrication. *Int. J. Nanoelectron. Mater.* **6**(2), 121–128 (2013).
73. Fakhri, M. A. *et al.* Optical investigation of nanophotonic lithium niobate-based optical waveguide. *Appl. Phys. B: Lasers Opt.* **121**(1), 107–116. https://doi.org/10.1007/s00340-015-6206-x (2015).
74. Abdul-Muhsien, M., Salim, E. T., Al-Douri, Y., Sale, A. F. & Agool, I. R. Synthesis of SnO2 nanostructures employing Nd:YAG laser. *Appl. Phys. A* **120**(2), 725–730. https://doi.org/10.1007/s00339-015-9249-2 (2015).
75. Koch, C. C., Ovid'Ko, I. A., Seal, S. & Veprek, S. *Structural Nanocrystalline Materials: Fundamentals and Applications* (Cambridge University Press, 2007).
76. Salim, E. T., Al-Douri, Y., Al-Wazny, M. S. & Fakhri, M. A. Optical properties of Cauliflower-like Bi2O3nanostructures by reactive pulsed laser deposition (PLD) technique. *Solar Energy* **107**, 523–529. https://doi.org/10.1016/j.solener.2014.05.020 (2014).
77. Swanson, W. E. *Tables for Conversion of X-ray Diffraction Angles to In-terplanar Spacing* (National Bureau of Standards, 1960).
78. Wang, T. *et al.* Structure and photoluminescence properties of the quasi-regular arrangements of porous silicon. *Optoelectron. Adv. Mater.-Rapid Commun.* **5**(2011), 495–498 (2011).
79. Salim, Z. T., Hashim, U., Arshad, M. K. M., Fakhri, M. A. & Salim, E. T. Zinc oxide flakes-corolla lobes like nano combined structure for SAW applications. *Mater. Res. Bull.* **86**, 215–219. https://doi.org/10.1016/j.materresbull.2016.11.015 (2017).
80. Fakhri, M. A. *et al.* Synthesis and characterization of nanostructured LiNbO3 films with variation of stirring duration. *J. Mater. Sci.: Mater. Electron.* **28**(16), 11813–11822. https://doi.org/10.1007/s10854-017-6989-0 (2017).
81. Hassanien, A. S. & Akl, A. A. Effect of Se addition on optical and electrical properties of chalcogenide CdSSe thin films. *Superlatt. Microstruct.s* **89**, 153–169 (2016).
82. Saxena, S. K. *et al.* Effect of silicon resistivity on its porosification using metal induced chemical etching: Morphology and photoluminescence studies. *Mater. Res. Express* **2**(3), 036501 (2015).

83. Salim, Z. T., Hashim, U., Arshad, M. KMd., Fakhri, M. A. & Salim, E. T. Frequency-based detection of female Aedes mosquito using surface acoustic wave technology: Early prevention of dengue fever. *Microelectron. Eng.* **179**, 83–90. https://doi.org/10.1016/j.mee.2017.04.016 (2017).
84. Salim, E. T., Saimon, J. A., Abood, M. K. & Fakhri, M. A. Some physical properties of Nb2O5 thin films prepared using nobic acid based colloidal suspension at room temperature. *Mater. Res. Express* **4**(10), 106407. https://doi.org/10.1088/2053-1591/aa90a6 (2017).
85. Fakhri, M. A. *et al.* Enhancement of Lithium Niobate nanophotonic structures via spin-coating technique for optical waveguides application. *Eur. Phys. J. Conf.* **162**(7), 01004. https://doi.org/10.1051/epjconf/201716201004 (2017).
86. Sultan, F. I., Slman, A. A. & Nayef, U. M. IV and CV characteristics of porous silicon nanostructures by electrochemical etching. *Eng. Technol. J.* **31**(3), 154 (2013).
87. Ismail, R. A., Habubi, N. F. & Abbod, M. M. Preparation of high-sensitivity In_2S_3/Si heterojunction photodetector by chemical spray pyrolysis. *Opt. Quant. Electron.* **48**, 1–14 (2016).
88. Fakhri, M. A., Al-Douri, Y., Bouhemadou, A. & Ameri, M. Structural and optical properties of nanophotonic LiNbO3 under stirrer time effect. *J. Opt. Commun.* **39**(3), 297–306. https://doi.org/10.1515/joc-2016-0159 (2017).
89. Abood, M. K., Salim, E. T. & Saimon, J. A. Impact of substrate type on the microstructure of H-Nb2o5 thin film at room temperature. *Int. J. Nanoelectron. Mater.* **11**(21), 55–64 (2018).
90. Pujadó, M. P. *Carbon Nanotubes as Platforms for Biosensors with Electrochemical and Electronic Transduction* (Springer Science & Business Media, 2012).
91. Hattab, F. & Fakhry, M. Optical and structure properties for nano titanium oxide thin film prepared by PLD. In *2012 1st Natl. Conf. Eng. Sci. FNCES 2012*, no. 6000 7–11 (2012). https://doi.org/10.1109/NCES.2012.6740474.
92. Abd, A. N., Habubi, N. F., Reshak, A. H. & Mansour, H. L. Enhancing the electrical properties of porous silicon photodetector by depositing MWCNTs. *Int. J. Nanoelectron. Mater.* **11**, 3 (2018).
93. Abood, M. K., Wahid, M. H. A., Saimon, J. A. & Salim, E. T. Physical properties of Nb2O5 thin films prepared at 12M ammonium concentration. *Int. J. Nanoelectron. Mater.* **11**, 237–244 (2018).
94. Hassan, M. A. M., Al-Kadhemy, M. F. H. & Salem, E. T. Effect irradiation time of Gamma ray on MSISM (Au/SnO2/SiO2/Si/Al) devices using theoretical modeling. *Int. J. Nanoelectron. Mater.* **8**(2), 69–82 (2014).
95. Fakhri, M. A. *et al.* Responsivity and response time of nano silver oxide on silicon heterojunction detector. *Int. J. Nanoelectron. Mater.* **11**, 109–114 (2018).
96. Abood, M. K., Wahid, M. H. A., Salim, E. T. & Saimon, J. A. Niobium pentoxide thin films employ simple colloidal suspension at low preparation temperature. *EPJ Web Conf.* **162**, 01508. https://doi.org/10.1051/epjconf/201716201058 (2017).
97. Ismail, R. A., Hasan, N. & Shaker, S. S. Preparation of Bi2Sr2CaCu2Ox thin film by pulsed laser deposition for optoelectronic devices application. *Silicon* **14**, 2625–2633 (2022).
98. Agool, I. R., Salim, E. T. & Muhsien, M. A. Optical and electrical properties of SnO2thin film prepared using RTO method. *Int. J. Modern Phys. B* **25**(8), 1081–1089 (2011).
99. Fakhri, M. A. *et al.* Enhancement of lithium niobate nanophotonic structures via spin-coating technique for optical waveguides application. *EPJ Web Conf.* **162**, 01004. https://doi.org/10.1051/epjconf/201716201004 (2017).
100. Halboos, H. T. & Salim, E. T. Silver doped niobium pentoxide nanostructured thin film, optical structural and morphological properties. *IOP Conf. Ser. Mater. Sci. Eng.* **454**(1), 012174. https://doi.org/10.1088/1757-899X/454/1/012174 (2018).
101. Narang, K. *et al.* Improvement in surface morphology and 2DEG properties of AlGaN/GaN HEMT. *J. Alloys Compd.* **815**, 152283 (2020).
102. Taha, J. M., Nassif, R. A., Numan, N. H. & Fakhri, M. A. Effects of oxygen gas on the physical properties of tin oxide nano films using laser light as ablation source. *AIP Conf. Proc.* **2213**, 144. https://doi.org/10.1063/5.0000198 (2020).
103. Yang, C. *et al.* High breakdown voltage and low dynamic ON-resistance AlGaN/GaN HEMT with fluorine ion implantation in SiNx passivation layer. *Nanoscale Res. Lett.* **14**(1), 1–6 (2019).
104. Salim, E. T., Ismail, R. A. & Halbos, H. T. Deposition geometry effect on structural, morphological and optical properties of Nb_2O_5 nanostructure prepared by hydrothermal technique. *Appl. Phys. A* **126**(11), 891 (2020).
105. Al-Wazny, M. S., Salim, E. T., Bader, B. A. & Fakhry, M. A. Synthesis of Bi2O3 films, studying their optical, structural, and surface roughness properties. *IOP Conf. Ser. Mater. Sci. Eng.* **454**(1), 012160. https://doi.org/10.1088/1757-899X/454/1/012160 (2018).
106. Ismail, R. A. "Fabrication and characterization of photodetector based on porous silicon. *e-J. Surf. Sci. Nanotechnol.* **8**, 388–391 (2010).
107. Hamd, S. S., Ramizy, A. & Ismail, R. A. Preparation of novel B4C nanostructure/Si photodetectors by laser ablation in liquid. *Sci. Rep.* **12**(1), 1–15 (2022).
108. Fakhri, M. A. *et al.* Efficiency enhancement of optical strip waveguide by the effect of heat treatment. *Optik* **180**, 768–774. https://doi.org/10.1016/j.ijleo.2018.12.006 (2019).
109. Hattab, F. A. & Hamed, E. K. Laser energy effects on optical properties of titanium di-oxide prepared by reactive pulsed laser deposition. *Eng. Tech. J.* **30**(1), 3104–3111 (2012).
110. Salim, E. T., Saimon, J. A., Abood, M. K. & Fakhri, M. A. Electrical conductivity inversion for Nb2O5 nanostructure thin films at different temperatures. *Mater. Res. Express* **6**(12), 126459. https://doi.org/10.1088/2053-1591/ab771c (2019).
111. Ismail, R. A., Rawdhan, H. A. & Ahmed, D. S. High-responsivity hybrid α-Ag2S/Si photodetector prepared by pulsed laser ablation in liquid. *Beilstein J. Nanotechnol.* **11**(1), 1596–1607 (2020).
112. Fakhri, M. A., Abdulwahhab, A. W., Kadhim, S. M., Alwazni, M. S. & Adnan, S. A. Thermal oxidation effects on physical properties of CuO2 thin films for optoelectronic application. *Mater. Res. Express* **6**(2), 026429 (2018).
113. Salim, E. T. *et al.* Effect of light induced heat treatment on the structural and morphological properties of LiNbO3 thin films. *Super Lattices Microstruct.* **128**, 67–75. https://doi.org/10.1016/j.spmi.2019.01.016 (2019).
114. Fakhri, M. A. *et al.* The effect of annealing temperature on optical and photolumence proper. *Surface Rev. Lett.* **26**(10), 1950068. https://doi.org/10.1142/S0218625X19500689 (2019).
115. Jiang, H. H. *et al.* GaN MSM structure UV photodetector detector based on nonplanar Si substrate and its performance optimization. *Semicond. Sci. Technol.* **37**(10), 105020 (2022).

Acknowledgements

The authors would like to thank the University of Technology-Iraq for the logistic support this work. The authors extend their appreciation to the Deanship of Scientific Research at Northern Border University, Arar, KSA for support this research work through the project number "NBU-FFR-2023-0139. The authors gratefully thank the Prince Faisal bin Khalid bin Sultan Research Chair in Renewable Energy Studies and Applications (PFCRE) at Northern Border University for their support and assistance. The authors would like to thank Al-Farahidi University, Baghdad, Iraq for the logistic support this work.

Author contributions

M.A.F., H.D.J., M.J.A., E.T.S., A.S.A., R.K.I., R.A.I., conceptualization, M.A.F., H.D.J., M.J.A., E.T.S; methodology, M.A.F., H.D.J., M.J.A., E.T.S; validation, M.A F., E.T.S., A.S.A., R.K.I., R.A.I.; formal analysis, M.A.F., H.D.J., M.J.A., E.T.S.; investigation, M.A.F., H.D.J., E.T.S., A.S.A., R.K.I., R.A.I.; resources, M.A.F., E.T.S., A.S.A., R.K.I., R.A.I.; data curation, M.A.F., H.D.J., E.T.S.; writing—original draft preparation, H.D.J.; writing—review and editing, M.A.F., M.J.A., E.T.S., A.S.A., R.K.I., R.A.I.; visualization, M.A.F., H.D.J., M.J.A., E.T.S., A.S.A., R.K.I., R.A.I.; supervision, M.A.F., M.J.A.; project administration, M.A.F., M.J.A., E.T.S.; funding acquisition, A.S.A., all authors have read and agreed to the published version of the manuscript.

Competing interests

The authors declare no competing interests.

Additional information

Correspondence and requests for materials should be addressed to M.A.F., E.T.S. or A.S.A.

Reprints and permissions information is available at www.nature.com/reprints.

Publisher's note Springer Nature remains neutral with regard to jurisdictional claims in published maps and institutional affiliations.

Open Access This article is licensed under a Creative Commons Attribution 4.0 International License, which permits use, sharing, adaptation, distribution and reproduction in any medium or format, as long as you give appropriate credit to the original author(s) and the source, provide a link to the Creative Commons licence, and indicate if changes were made. The images or other third party material in this article are included in the article's Creative Commons licence, unless indicated otherwise in a credit line to the material. If material is not included in the article's Creative Commons licence and your intended use is not permitted by statutory regulation or exceeds the permitted use, you will need to obtain permission directly from the copyright holder. To view a copy of this licence, visit http://creativecommons.org/licenses/by/4.0/.

© The Author(s) 2023